



# Analysis of the seismicity in central Tibet based on the SANDWICH network and its tectonic implications



Gaohua Zhu<sup>a,b,c</sup>, Xiaofeng Liang<sup>a</sup>, Xiaobo Tian<sup>a,d,\*</sup>, Hongfeng Yang<sup>c</sup>, Chenglong Wu<sup>a,b</sup>, Yaohui Duan<sup>a,b</sup>, Wei Li<sup>a,b</sup>, Beibei Zhou<sup>a,b</sup>

<sup>a</sup> State Key Laboratory of Lithospheric Evolution, Institute of Geology and Geophysics, Chinese Academy of Sciences, Beijing 100029, China

<sup>b</sup> University of Chinese Academy of Sciences, Beijing 100049, China

<sup>c</sup> Earth System Science Programme, Faculty of Science, Chinese University of Hong Kong, Hong Kong

<sup>d</sup> CAS Center for Excellence in Tibetan Plateau Earth Sciences, Beijing 100101, China

## ARTICLE INFO

### Article history:

Received 4 February 2017

Received in revised form 20 February 2017

Accepted 22 February 2017

Available online 24 February 2017

### Keywords:

Central Tibetan Plateau

Conjugate strike-slip faults

Seismicity

Crustal deformation

## ABSTRACT

We have located a total of 232 local earthquakes using data recorded by the SANDWICH seismic network from November 2013 to October 2014 in central Tibet across the Bangong–Nujiang suture (BNS). The focal depths of all earthquakes are shallower than 30 km and therefore are in the upper crust. The absence of lower crust earthquakes may imply a weak, ductile lower crust in central Tibet. Moreover, these earthquakes are dispersed throughout conjugate strike-slip fault zones, indicating that evenly distributed upper crustal deformation might predominate in central Tibet. This observation agrees with the hypothesis that conjugate fault zones accommodate coeval east–west extension and north–south contraction via continuous deformation. Moreover, the focal mechanisms show that strike-slip and normal faulting are the dominant types of deformation and that the extension in central Tibet is oriented approximately east–west. Despite some anomalies, the kinematics implied by most of the focal mechanisms correlate well with those of the surface structures.

© 2017 Elsevier B.V. All rights reserved.

## 1. Introduction

The Tibetan Plateau was formed by the collision between the Indian and Eurasian plates (Molnar and Tapponnier, 1978). Consequently, the collision zone features well-developed large-scale thrust faults and frequent large earthquakes, such as the 2015 Mw 7.8 Gorkha earthquake (e.g., Yin et al., 2016). Despite the intense compressive stress, the most striking geologic structures in central and southern Tibet are a series of nearly north–south-trending rifts (Fig. 1) at elevations above 4000 m (Molnar et al., 1993). The development of north–south-trending rifts in southern Tibet began in the mid-to-late Miocene (18–8 Ma) (Coleman and Hodges, 1995) as the result of extension or eastward extrusion (Armijo et al., 1986; Armijo et al., 1989; Styron et al., 2011). Associated with the rifts, a series of conjugate strike-slip faults also developed and are thought to accommodate coeval east–west extension and north–south contraction (Taylor et al., 2003). Understanding how extensional rifts formed in such a large-scale compressional setting holds important implications for the evolution of the Tibetan Plateau.

Several mechanisms responsible for the east–west extension have been proposed. Based on observations of widespread normal faulting at high elevations throughout the plateau (Molnar and Tapponnier, 1978; Molnar et al., 1993), gravitational collapse has been suggested as one of the mechanisms. This mechanism implies that the age of the initiation of the rifts should agree with the timing of rapid uplift of the Tibetan Plateau at approximately 8 Ma (Harrison et al., 1992; Molnar et al., 1993). However, the onset of rifting in southern Tibet is estimated to have commenced between 18 Ma and 8 Ma (Coleman and Hodges, 1995), and the onset of graben formation in central Tibet is estimated to have occurred at >13.5 Ma based on mineralization ages (Blisniuk et al., 2001). Alternatively, convective removal of Tibetan mantle lithosphere (England and Houseman, 1989; Molnar et al., 1993) has been proposed to explain not only the rapid uplift but also the basaltic volcanism in northern Tibet at ~13 Ma (Turner et al., 1993). However, because the modeled east–west extension rate is generally slower than the observed values, a lower crustal flow model has been proposed based on GPS observations of crustal deformation (Royden et al., 1997). This model also suggests that the surface deformation is strongly decoupled from the lower crust. More recently, a series of studies using newly acquired seismic data suggest that asthenospheric upwelling from a slab window has significantly contributed to the extension pattern in southern Tibet and that the separation between surface rifting and Moho uplift is likely due to partial decoupling across the ductile

\* Corresponding author at: State Key Laboratory of Lithospheric Evolution, Institute of Geology and Geophysics, Chinese Academy of Sciences, Beijing 100029, China.

E-mail address: [txb@mail.iggcas.ac.cn](mailto:txb@mail.iggcas.ac.cn) (X. Tian).

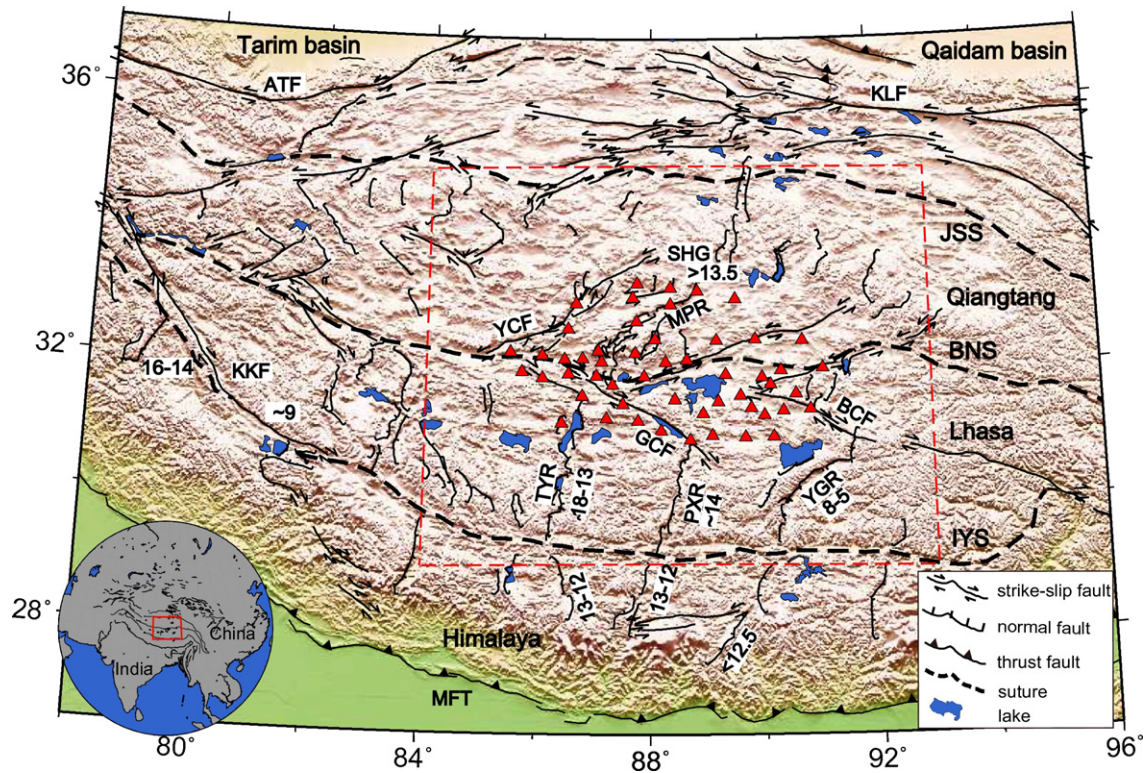


**Fig. 1.** A map showing study area (red box) and the location of the SANDWICH seismic network (red triangles). The location of active faults and sutures is from the HimaTibetMap database (Styron et al., 2010). Abbreviations of major geological structures: JSS = JinSha Suture, BNS = Bangong-Nujiang Suture, IYS = Indus-Yalu Suture, ATF = Altyr Tagh fault, KLF = Kunlun fault, SHG = Shuang Hu graben, YCF = Yibug Caka fault, MPR = Muga-Puruo rift, GCF = Gyaring Co fault, BCF = BangCo fault, YGR = Yadong-Gulu rift, PXR = Pumqu-Xianza rift, TYR = Tangra Yum Co rift, KKF = Karakoram fault, MFT = Main Frontal thrust (Lee et al., 2011; Taylor and Yin, 2009). The numbers represent the initiation ages (Ma) of the faults (Lee et al., 2011; Styron et al., 2011; Sundell et al., 2013).

middle crust (Chen et al., 2015; Liang et al., 2016a; Tian et al., 2015). However, whether the rifts are restricted to the upper crust or penetrate through the entire lithosphere is still under debate (Yin, 2000).

Seismicity analysis is a good method for identifying the style of active crustal deformation. Specifically, the depth of seismicity can be a good indicator of whether the deformation is limited to the upper crust or extends to greater depths. For example, earthquakes in northeastern and central Tibet are mainly distributed in the upper crust at depths shallower than 25 km (Wei et al., 2010; Zhao and Helmlinger, 1991; Langin et al., 2003). In stark contrast, earthquakes with focal depths in the upper mantle ( $>70$  km) have been found in southern Tibet using waveform modeling (Zhu and Helmlinger, 1996). Due to the scarcity of seismic stations in Tibet, most of these earthquakes have been located using teleseismic or regional waveforms, and their spatial distribution may therefore contain some degree of uncertainty. In this study, we investigate earthquakes in the rift and strike-slip fault systems in central Tibet using broadband seismic waveforms recorded by a newly deployed seismic network. We first detect and locate local earthquakes. Then, we derive focal mechanisms for earthquakes with magnitudes  $>3.4$ . Our results offer better observational evidences for the seismogenic depth, the distribution of active faulting related to the seismicity, and the mechanism responsible for active crustal deformation in central Tibet.

## 2. Tectonic setting and data

The conjugate strike-slip faults in central Tibet are evenly distributed on both sides of the Bangong-Nujiang suture (BNS), which separates the Qiangtang terrane and the Lhasa terrane (Fig. 1). In the Qiangtang terrane north of the BNS, all the strike-slip faults are left lateral with

northeast strikes. In contrast, to the south of the BNS, the faults are right lateral with northwest strikes (Armijo et al., 1986; Taylor et al., 2003). A series of north-south-trending rifts are located to the south and north of this conjugate strike-slip fault zone, especially to the south (Taylor and Yin, 2009). In our research region, the three large-scale rifts in the Lhasa terrane from east to west are the Yadong Gulu rift (YGR), Pumqu Xianza rift (PXR) and Tangra Yum Co rift (TYR). In the Qiangtang terrane, the major rifts are the Muga-Puruo rift (MPR) and Shuang Hu graben (SHG). The structures identified in this study are from the HimaTibetMap dataset, which has collected data from academic journals, remote sensing interpretations, and other information (e.g., seismic focal mechanisms) (Taylor et al., 2003; Styron et al., 2010).

Focal mechanisms from the Global Centroid Moment Tensor (GCMT) catalog show that most of normal faulting earthquakes were clustered near the rifts but that some strike-slip earthquakes occurred relatively far from the conjugate strike-slip faults (Fig. 2). Earthquake locations from the E.R. Engdahl, Van der Hilst, R.D., and Buland, R.P. (EHB) bulletin are mostly associated with reported rifts or faults (Fig. 2). Note that the vast majority of focal mechanisms are associated with either normal or strike-slip faulting. However, two earthquakes with thrust mechanisms occurred in our study region.

To investigate the tectonic features and seismogenic properties of the region, we have deployed a temporary seismic network, the SANDWICH (Seismic Array iNtegrated Detection for a Window of Indian Continental Head) network. This deployment represents the first seismic network operated in central Tibet, partly due to the harsh natural environment and limited financial support for instrumentation (Liang et al., 2016b). The SANDWICH network consists of 53 intermediate-band and broadband seismometers equipped with three-component Guralp CMG-3ESP sensors, with a response band from 60/30 s to 50 Hz. The

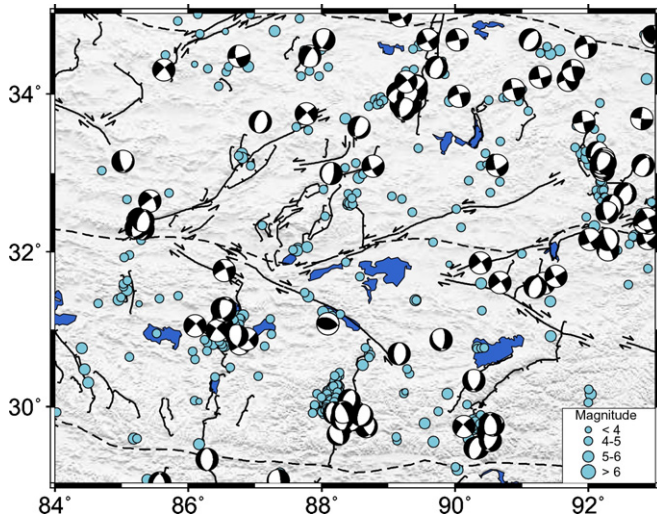


**Fig. 2.** Map of historical earthquake locations (from EHB Bulletin, 1961–2008) and historical focal mechanisms (GCMT solutions, 1976–2015) in central Tibet. The light blue circles indicate earthquake locations and are scaled by magnitude.

digital recorders are RefTek 72A-8/130-1 or DAS24-3D (Liang et al., 2016b). The network covers both sides of the BNS from the northern Lhasa terrane to the southern Qiangtang terrane (Fig. 1). The average inter-station distance is approximately 40 km. The data are recorded in three components with 40 samples per second.

The SANDWICH network began recording in early November 2013 and is expected to finish in November 2017. The waveform data recorded by the array provide an unprecedented opportunity for us to investigate the high-resolution spatial and temporal patterns of local seismicity. In this study, we use the first-phase waveform data from the end of November 2013 to the end of October 2014. Fig. 3 shows a cross section of the waveforms for a local  $M_L$  4.1 earthquake.

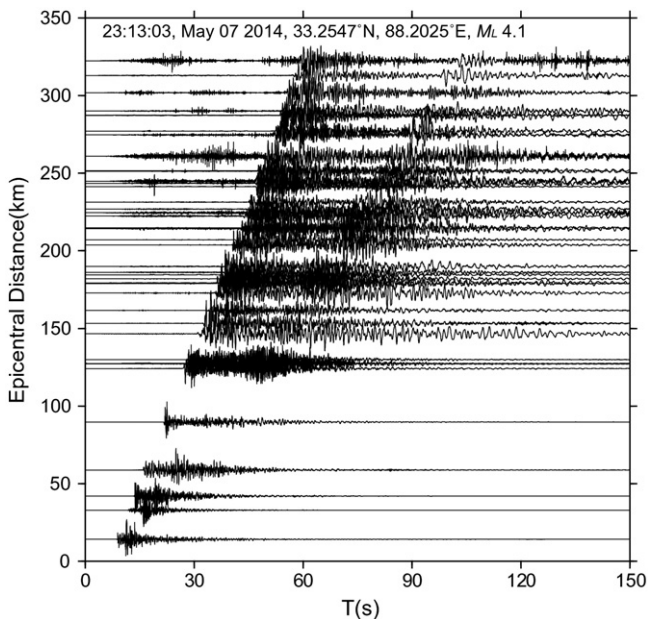


**Fig. 3.** Vertical-component waveforms of a local earthquake, whose location is shown in Fig. 4(a).

### 3. Results

#### 3.1. Earthquake detection and location

Because of the deficiency of permanent seismic stations in central Tibet, the earthquake catalog is generally incomplete. Thus, we first detected earthquakes using an event detection algorithm based on the ratio of the short-term average (STA) to the long-term average (LTA) (Freiberger, 1963; Earle and Shearer, 1994). Here, we used 10 s and 60 s as the short-term and the long-term windows, respectively. The critical triggered STA/LTA ratio is 3.5 over at least 13 stations. After visually inspecting the detected events and discarding the false detections, we eventually identified 232 local earthquakes in the one-year dataset.

We then located these earthquakes using Hypoinverse2000 (Klein, 2012). P and S phases were manually picked using Seismic Analysis Code (SAC). To avoid possible time shifts in phases caused by filtering effects, we picked most of the arrivals from raw waveforms. For noisy data, we applied a 0.5–5 Hz bandpass filter. A 1-D layered velocity model adopted from CRUST1.0 (Table 1) was used to locate the earthquakes (Laske et al., 2013). On average, the uncertainties in the horizontal locations of our located earthquakes are  $< 1$  km, thereby allowing us to reliably correlate these earthquakes to known surface faults. The located earthquakes have magnitudes ranging from  $M_L$  1.6 to 5.3, and the earthquakes with magnitudes larger than  $M_L$  5.0 are well correlated with known normal and strike-slip faults in the region (Fig. 4).

Several earthquake clusters are present in our research area and are clearly consistent with existing faults. For instance, the largest cluster contains 29 earthquakes near  $33.8^\circ\text{N}$ ,  $89.2^\circ\text{E}$ , in the vicinity of the SHG (Fig. 4a, cluster A). These earthquakes are located in a narrow north-south-trending area that is located 5–10 km west of the mapped fault (Fig. 4b). The largest earthquake,  $M_L$  5.2, occurred on February 11, 2014, and was preceded by 4 foreshocks and followed by 10 immediate aftershocks on the same day. Moreover, cluster B contains 17 earthquakes, is located near  $31.4^\circ\text{N}$ ,  $86.5^\circ\text{E}$  (Fig. 4a), and coincides with the northern section of the TYR, which intersects with a branch of a conjugate strike-slip fault at its north end. Furthermore, a cluster of 9 earthquakes near  $32.0^\circ\text{N}$ ,  $90.2^\circ\text{E}$  (Fig. 4a, cluster C) appears to be associated with a northeast-trending strike-slip fault.

In contrast, a few earthquakes are poorly correlated with mapped faults (Fig. 4a). We quantified the shortest distance from an earthquake to the nearest fault, i.e., the surface distance between a fault and the earthquake epicenter normal to the fault line (Fig. 5). Nearly 80% of these earthquakes are located within a 6-km normal distance of a fault. If we only consider earthquakes with horizontal uncertainties of  $< 3$  km, 80% of earthquakes remain in the same range (Fig. 5a).

We also investigated the depth distribution of these earthquakes. Compared to the uncertainties in the horizontal locations, the uncertainties in the focal depths for some earthquakes are much larger, e.g., several to tens of kilometers (Fig. 6). However, all the earthquakes are located at depths no  $> 30$  km (Fig. 6c), i.e., the upper to middle crust. Nearly half of the events are located at depths of 5–10 km.

#### 3.2. Focal mechanisms

We determined focal mechanisms for a number of earthquakes using the Computer Programs in Seismology (CPS) package

**Table 1**  
Earth structure model.

Depth km	P km/s	S km/s	Density g/cm <sup>3</sup>
0	5.3	3.0	2.5
4	6.1	3.5	2.7
29	6.7	3.8	2.8
64	7.9	4.5	3.2

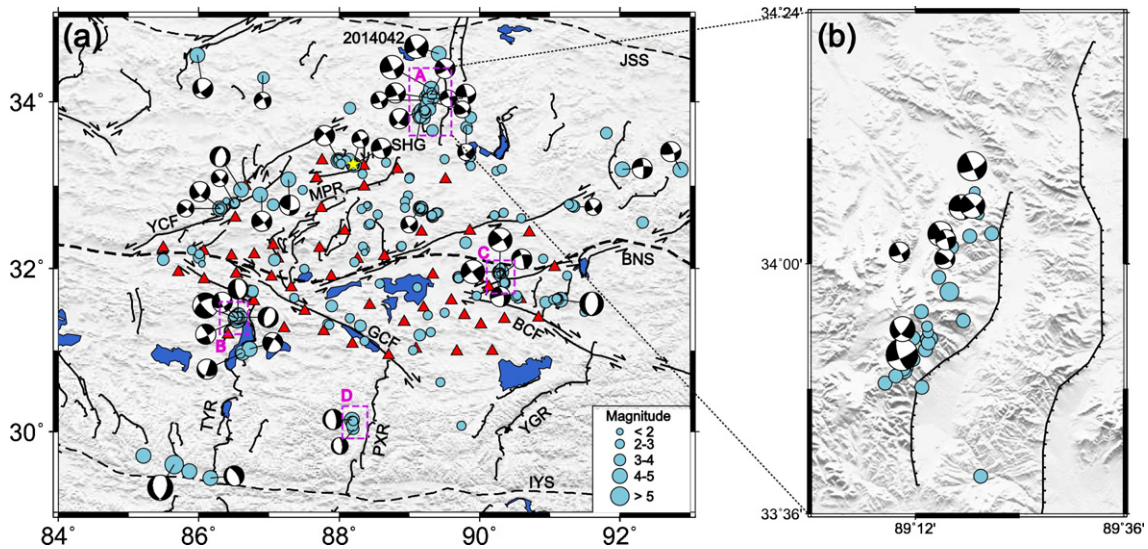


**Fig. 4.** (a) Map of earthquake locations (blue circles) and focal mechanisms from this study. The yellow star shows the location of the  $M_L$  4.1 earthquake in Fig. 3. (b) Zoom in map of earthquakes in the vicinity of the SHG, showing an enlarged view of cluster A in Fig. 4(a).

(Herrmann et al., 2011a; Herrmann et al., 2011b; Herrmann, 2013). We first converted the raw digital waveform data to ground velocity (m/s) after removal of the instrument response and then rotated the two horizontal components to radial and transverse orientations. For most of earthquakes, we applied a Butterworth bandpass filter of 0.02–0.1 Hz, but for events with low signal-to-noise ratios, we applied a bandpass filter of 0.02–0.08 Hz or 0.02–0.06 Hz. The source mechanism was obtained by applying a grid search in the parameter space (strike, dip, rake, and depth) to find the best fit between synthetic and observed waveforms. The waveform comparison and depth sensitivity for an  $M_L$  4.9 earthquake are shown in Supplementary Figs. 1 and 2, respectively.

In the end, 42 focal mechanisms with high-quality inversion results and minimal magnitudes of  $M_L$  3.4 have been obtained (Fig. 4). To the south of the BNS, the earthquake focal mechanisms indicate the presence of both normal (e.g., cluster D near the PXR) and strike-slip faulting (e.g., cluster C), as well as oblique events (e.g., cluster B). To the north of the BNS, however, most of the focal mechanisms indicate the presence of strike-slip faulting (Fig. 4a). Generally, most of the mechanisms are

in good agreement with the long-term movement of the mapped faults. For example, earthquakes along the left-lateral strike-slip faults associated with the Yibug Caka Fault (YCF) and the MPR exhibit strike-slip mechanisms. However, some observations are not exactly consistent with the mapped surface features. The most peculiar observation is a cluster of earthquakes with strike-slip mechanisms immediately west of a normal fault in the SHG (Fig. 4b).

#### 4. Discussion

The thickness of the seismogenic layer has been taken as a proxy for the crustal rheological and thermal structure and the strength of the continental lithosphere. The limiting temperature of material in which crustal earthquakes occur is approximately  $350 \pm 100$  °C, equivalent to a depth of approximately  $25 \pm 5$  km (Chen and Molnar, 1983). This temperature has been used to discuss the elastic thickness of the continental crust (Maggi et al., 2000).

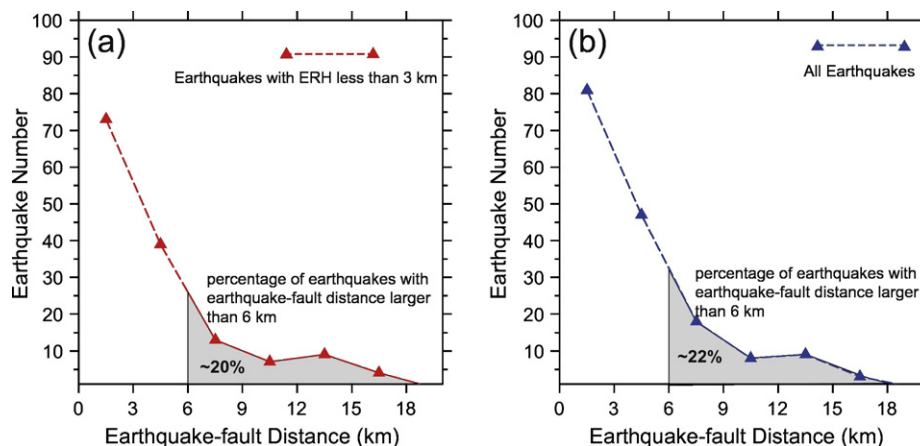


**Fig. 5.** (a) Event-fault distance distribution for events with horizontal errors  $< 3$  km within the SANDWICH array. (b) Event-fault distance distribution for all events within the SANDWICH array. The numbers in the gray shading represent the percentages of events with event-fault distances  $> 6$  km.

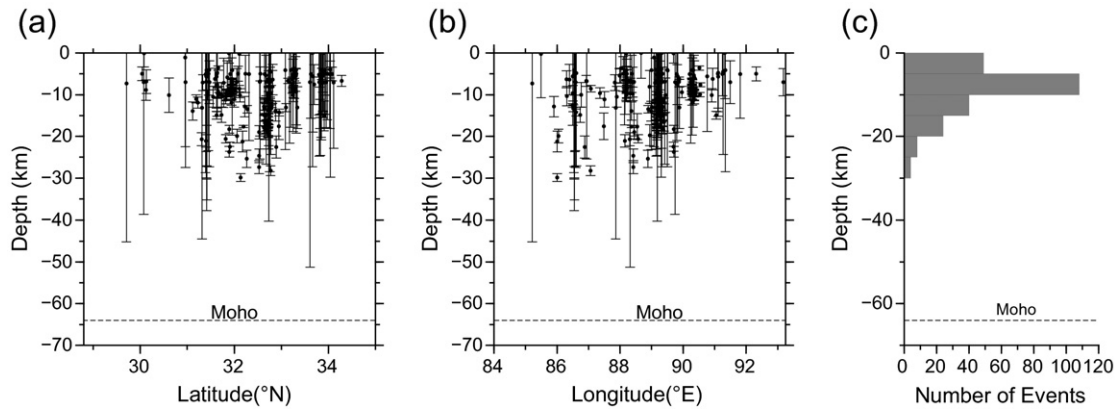


**Fig. 6.** The depth distribution of the earthquakes in this study. Focal depths with corresponding vertical uncertainties along latitude (a) and longitude (b). (c) Histogram of the depth distribution of earthquakes located in this study.

In our study region, we observed no earthquakes in the lower crust or upper mantle, which is different from southern Tibet, where two seismogenic layers exist: the upper crust and the uppermost mantle (Liang et al., 2008; Zhu and Helmberger, 1996). Therefore, based on our observations, central Tibet contains only one seismogenic layer in the upper crust. The absence of lower crustal and upper mantle earthquakes may indicate a ductile lower crust and upper mantle in central Tibet.

Our observations are consistent with the low-velocity layer below 20 km depth in the Lhasa terrane (Owens and Zandt, 1997; Yuan et al., 1997), low crustal  $V_s$  and high  $V_p/V_s$  values within the mid-lower crust (Owens and Zandt, 1997; Tian et al., 2005), and high conductivities in the northern Lhasa terrane and Qiangtang terrane (Chen et al., 1996; Pham et al., 1986). The lack of lower crust and upper mantle earthquakes is also coincident with strong crustal attenuation (Zhao et al., 2013), significantly lower  $P_n$  velocities in this region (Liang et al., 2004), and localized asthenospheric upwelling under northern Tibet (Liang et al., 2016a; Tilmann et al., 2003). Overall, our results are highly consistent with these studies and support the existence of a weak and ductile lower crust and upper mantle beneath central Tibet.

Moreover, a weak and ductile lower crust in central Tibet may support the hypothesis that the Tibetan lower crust is capable of flowing laterally (Royden, 1996; Royden et al., 1997; Clark and Royden, 2000). This lateral flow may be responsible for the formation of the conjugate strike-slip faults in central Tibet (Yin and Taylor, 2011). Two analogue experiments suggest that the basal shear imposed by flow in the lower crust or asthenosphere could produce conjugate strike-slip faults in central Tibet and that eastward mid-crustal flow along a flow axis parallel to the BNS could generate the required basal shear (Yin and Taylor, 2011). Thus, our results may demonstrate the feasibility of the basal shear mechanism for the formation of the conjugate strike-slip faults in central Tibet.

Additionally, debate has long focused on how the intracontinental deformation accommodates Indo-Asian contraction. According to the lateral extrusion hypothesis, the blocks are rigid and relatively undeformed and significant slip occurs along large-scale strike-slip faults (Tapponnier et al., 2001). In contrast, some studies propose continuous deformation of the upper crust (Zhang et al., 2004) or the entire lithosphere (Houseman and England, 1993). If the regional deformation is characterized by the relative movement of rigid blocks, we expect that most of earthquakes would occur near major faults. However, ~20% earthquakes in conjugate strike-slip fault zones are dispersed throughout the region, without obvious correlation with any known major active faults. Therefore, although the strain energy is mainly released by movement along major tectonic faults, a significant component of diffused energy is released by unmapped minor faults in the conjugate

strike-slip fault zone. This observation may imply that continuous deformation is occurring in the Tibetan upper crust or throughout the entire lithosphere (Tian et al., 2015), which is consistent with GPS observations (Zhang et al., 2004).

The focal mechanisms show that strike-slip and normal faulting are the dominant types of deformation in central Tibet. Both the normal faulting and strike-slip faulting indicate that the tectonic regime in the central Tibetan Plateau is extensional. Despite a few anomalous results, the focal mechanisms in this study generally indicate that the central Tibetan Plateau is extending in an approximately east-west direction. The consistency between the seismological focal mechanisms and tectonic background suggests that the seismogenic processes are controlled by the regional background stress.

The contradiction between the geologic evidence of normal faulting and the strike-slip focal mechanisms in the SHG may be due to several possible reasons. First, the precision of the fault locations is suitable for regional-scale mapping but may be inaccurate at smaller scales (Taylor et al., 2003; Styron et al., 2010). On the other hand, if the location of the normal faults is correct, the contradiction might be attributable to the differences between regional long-term deformation and recent crustal deformation. Rifts represent the long-term integration of normal fault movement rather than the instantaneous strike-slip movement of an earthquake on a fault plane. Moreover, the discrepancy might imply a recent transition in the local geologic deformation process. The SHG appears to be kinematically associated with the MPR, which is experiencing a localized combination of strike-slip and normal faulting (Taylor et al., 2003). Therefore, this discrepancy might represent the possible interaction between a conjugate strike-slip fault zone and normal rifts.

Alternatively, previous studies have demonstrated that the extensional rates are distinct in different parts of Tibet (Molnar and Lyon-Caen, 1989; Zhang et al., 2004) and displacements along different faults may vary (Elliott et al., 2010; Taylor et al., 2003). Thus, we surmise that the north-south-trending SHG is likely broken by a dislocation, which is akin to a transform fault or an accommodation zone (Fig. 7). Such strike-slip accommodation zone has been found in southern Illinois, where the 2008 Mw5.2 Mount Carmel strike-slip earthquake occurred between a series of well-known normal faults (Yang et al., 2009). Movement along the dislocation tends to express strike-slip characteristics, while movement along the master fault exhibits normal slip. The dislocation could express two possible trends, northeast-southwest (Fig. 7a) or northwest-southeast (Fig. 7b). Considering the northeast-southwest trend of the epicentral locations (Fig. 4b), the dislocation likely exhibits a northeast-southwest trend. Whether there is a strike-slip fault between the different normal fault segments demands further field investigation.

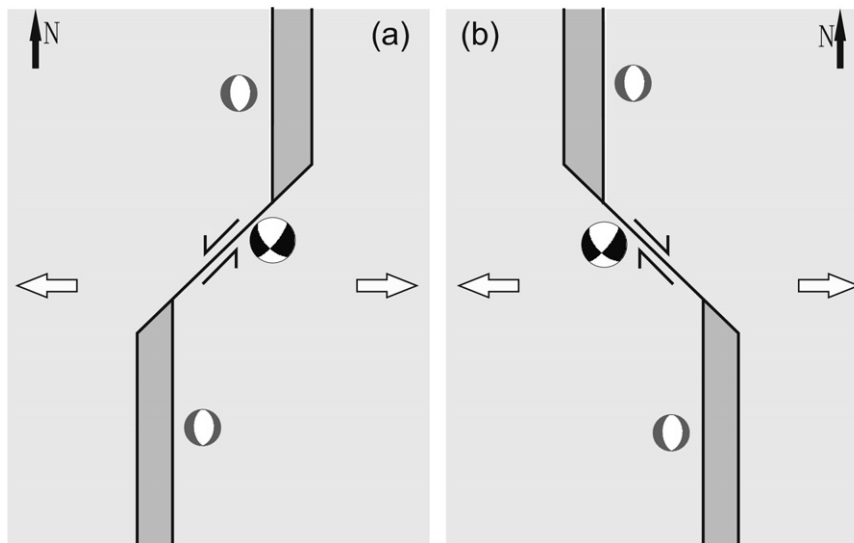


Fig. 7. Cartoon model illustrating the possible mechanism responsible for movement along a normal fault separated by a dislocation: (a) dislocation with a northeast-southwest trend; (b) dislocation with a northwest-southeast trend.

## 5. Conclusions

In this study, we use the first-phase waveform data recorded by the SANDWICH seismic network and focus on local earthquakes to investigate the detailed seismicity characteristics and the relationships between seismicity and regional tectonics in central Tibet.

In total, we have located 232 local small to moderate earthquakes occurring between the end of November 2013 and the end of October 2014. The earthquakes in this study occurred at depths shallower than 30 km and primarily at depths of 5–10 km, demonstrating that the upper crust contains the only seismogenic layer in central Tibet. The absence of lower crust earthquakes may suggest that a weak, ductile lower crust underlies central Tibet. Moreover, ~20% of the earthquakes are distributed in conjugate strike-slip fault zones and do not correspond well with known major faults. These observations are consistent with the existence of continuous upper crustal deformation in central Tibet.

Additionally, we have computed focal mechanisms for 42 earthquakes with magnitudes larger than  $M_L$  3.4. The focal mechanisms show that strike-slip and normal faulting are the dominant types of deformation and that extension is occurring in an approximately east-west direction in central Tibet. The majority of the observations are consistent with the kinematics of the surface geologic structures.

Supplementary data to this article can be found online at <http://dx.doi.org/10.1016/j.tecto.2017.02.020>.

## Acknowledgements

We would like to express our appreciation to Zhongjie Zhang, who passed away suddenly on September 6, 2013. Without his efforts, the SANDWICH project would not have been possible. We also thank all the members of the SANDWICH field team who collected the data used in our study. Qi-Fu Chen has provided helpful suggestions for the seismicity analysis. Computer Programs in Seismology package (Herrmann et al., 2011a; Herrmann et al., 2011b), Hypoinverse2000 (Klein, 2012), Generic Mapping Tools (Wessel and Smith, 1991), and PSSAC (developed by Prof. Lupei Zhu) were used for data analysis and figure preparation in our study. This research has been financially supported by Strategic Priority Research Program (B) of Chinese Academy of Sciences (grant XDB03010700), the National Key Research and Development Project of China (grant 2016YFC0600301), National Natural Science Foundation of China (grants 41574048, 41404051, 41274090 and 41574056) and Hong Kong SAR Research Grant Council (grants 2191093 and 2130509) as well as NSFC/RGC Joint Research Scheme

(Project No. N\_CUHK430/16). The authors appreciate constructive comments from two anonymous reviewers and the editor.

## References

- Armijo, R., Tapponnier, P., Mercier, J.L., Han, T., 1986. Quaternary extension in southern Tibet: field observations and tectonic implications. *J. Geophys. Res.* 91, 13803–13872.
- Armijo, R., Tapponnier, P., Han, T., 1989. Late Cenozoic right-lateral strike-slip faulting in southern Tibet. *J. Geophys. Res.* 94, 2787–2838.
- Blisniuk, P.M., Hacker, B.R., Glodny, J., Ratschbacher, L., Bi, S., Wu, Z., McWilliams, M.O., Calvert, A., 2001. Normal faulting in central Tibet since at least 13.5[thinsp]Myr ago. *Nature* 412, 628–632.
- Chen, L., Booker, J.R., Jones, A.G., Wu, N., Unsworth, M.J., Wei, W., Tan, H., 1996. Electrically conductive crust in southern Tibet from INDEPTH magnetotelluric surveying. *Science* 274, 1694–1696.
- Chen, W., Molnar, P., 1983. Focal depths of intracontinental and intraplate earthquakes and their implications for the thermal and mechanical properties of the lithosphere. *J. Geophys. Res.* 88, 4183–4214.
- Chen, Y., Li, W., Yuan, X., Badal, J., Teng, J., 2015. Tearing of the Indian lithospheric slab beneath southern Tibet revealed by SKS-wave splitting measurements. *Earth Planet. Sci. Lett.* 413, 13–24.
- Clark, M.K., Royden, L.H., 2000. Topographic ooze: building the eastern margin of Tibet by lower crustal flow. *Geology* 28, 703–706.
- Coleman, M., Hodges, K., 1995. Evidence for Tibetan plateau uplift before 14 Myr ago from a new minimum age for east-west extension. *Nature* 374, 49–52.
- Earle, P.S., Shearer, P.M., 1994. Characterization of global seismograms using an automatic-picking algorithm. *Bull. Seismol. Soc. Am.* 84, 366–376.
- Elliott, J.R., Walters, R.J., England, P.C., Jackson, J.A., Li, Z., Parsons, B., 2010. Extension on the Tibetan plateau: recent normal faulting measured by InSAR and body wave seismology. *Geophys. J. Int.* 183, 503–535.
- England, P., Houseman, G., 1989. Extension during continental convergence, with application to the Tibetan Plateau. *J. Geophys. Res.* 94, 17561.
- Freiberger, W.F., 1963. An approximation method in signal detection. *Quart. J. Appl. Math.* 20, 373–378.
- Harrison, T.M., Copeland, P., Kidd, W.S.F., Yin, A., 1992. Raising Tibet. *Science* 255, 1663–1670.
- Herrmann, R.B., Benz, H., Ammon, C.J., 2011a. Monitoring the earthquake source process in north America. *Bull. Seismol. Soc. Am.* 101, 2609–2625.
- Herrmann, R.B., Malagnini, L., Munafo, I., 2011b. Regional moment tensors of the 2009 L'Aquila earthquake sequence. *Bull. Seismol. Soc. Am.* 101, 975–993.
- Herrmann, R.B., 2013. Computer programs in seismology: an evolving tool for instruction and research. *Seism. Res. Lett.* 84, 1081–1088.
- Houseman, G., England, P., 1993. Crustal thickening versus lateral expulsion in the Indian-Asian continental collision. *J. Geophys. Res.* 98, 12233–12249.
- Klein, F.W., 2012. User's guide to HYPOINVERSE-2000, a Fortran program to solve for earthquake locations and magnitudes. U.S. Geol. Surv. Open File Rep. 02-171, 01–113.
- Langin, W.R., Brown, L.D., Sandvol, E.A., 2003. Seismicity of central Tibet from project INDEPTH III seismic recordings. *Bull. Seismol. Soc. Am.* 93, 2146–2159.
- Laske, G., Masters, G., Ma, Z., Pasyanos, M., 2013. Update on CRUST1.0 - a 1-degree global model of earth's crust. *Geophys. Res. Abstr.* 15, EGU2013-EGU2658.
- Lee, J., Hager, C., Wallis, S.R., Stockli, D.F., Whitehouse, M.J., Aoya, M., Wang, Y., 2011. Middle to late Miocene extremely rapid exhumation and thermal reequilibration in the Kung Co rift, southern Tibet. *Tectonics* 30, TC2007.
- Liang, C., Song, X., Huang, J., 2004. Tomographic inversion of Pn travel times in China. *J. Geophys. Res.* 109, B11304.

- Liang, X., Chen, Y., Tian, X., Chen, Y.J., Ni, J., Gallegos, A., Klemperer, S.L., Wang, M., Xu, T., Sun, C., Si, S., Lan, H., Teng, J., 2016b. 3D imaging of subducting and fragmenting Indian continental lithosphere beneath southern and central Tibet using body-wave finite-frequency tomography. *Earth Planet. Sci. Lett.* 443, 162–175.
- Liang, X., Tian, X., Zhu, G., Wu, C., Duan, Y., Li, W., Zhou, B., Zhang, M., Yu, G., Nie, S., Wang, G., Wang, M., Wu, Z., Liu, Z., Guo, X., Zhou, X., Wei, Z., Xu, T., Zhang, X., Bai, Z., Chen, Y., Teng, J., 2016a. SANDWICH: a 2D broadband seismic array in central Tibet. *Seismol. Res. Lett.* 87, 1–12.
- Liang, X., Zhou, S., Chen, Y.J., Jin, G., Xiao, L., Liu, P., Fu, Y., Tang, Y., Lou, X., Ning, J., 2008. Earthquake distribution in southern Tibet and its tectonic implications. *J. Geophys. Res.* 113, B12409.
- Maggi, A., Jackson, J.A., McKenzie, D., Priestley, K., 2000. Earthquake focal depths, effective elastic thickness, and the strength of the continental lithosphere. *Geology* 28, 495–498.
- Molnar, P., England, P., Martinod, J., 1993. Mantle dynamics, uplift of the Tibetan Plateau, and the Indian monsoon. *Rev. Geophys.* 31, 357–396.
- Molnar, P., Lyon-Caen, H., 1989. Fault plane solutions of earthquakes and active tectonics of the northern and eastern parts of the Tibetan Plateau. *Geophys. J. Int.* 99, 123–153.
- Molnar, P., Tapponnier, P., 1978. Active tectonics of Tibet. *J. Geophys. Res.* 83, 5361–5375.
- Owens, T.J., Zandt, G., 1997. Implications of crustal property variations for models of Tibetan plateau evolution. *Nature* 387, 37–43.
- Pham, V.N., Boyer, D., Therme, P., Yuan, X.C., Li, L., Jin, G.Y., 1986. Partial melting zones in the crust in southern Tibet from magnetotelluric results. *Nature* 319, 310–314.
- Royden, L., 1996. Coupling and decoupling of crust and mantle in convergent orogens: implications for strain partitioning in the crust. *J. Geophys. Res.* 101, 17679–17705.
- Royden, L.H., Burchfiel, B.C., King, R.W., Wang, E., Chen, Z., Shen, F., Liu, Y., 1997. Surface deformation and lower crustal flow in eastern Tibet. *Science* 276, 788–790.
- Styron, R., Taylor, M., Okoronkwo, K., 2010. Database of active structures from the Indo-Asian collision. *Trans. Am. Geophys. Union* 91, 181–182.
- Styron, R.H., Taylor, M.H., Murphy, M.A., 2011. Oblique convergence, arc-parallel extension, and the role of strike-slip faulting in the high Himalaya. *Geosphere* 7, 582–596.
- Sundell, K.E., Taylor, M.H., Styron, R.H., Stockli, D.F., Kapp, P., Hager, C., Liu, D.L., Ding, L., 2013. Evidence for constriction and Pliocene acceleration of east-west extension in the North Lunggar rift region of west central Tibet. *Tectonics* 32, 1454–1479.
- Tapponnier, P., Zhiqin, X., Roger, F., Meyer, B., Arnaud, N., Wittlinger, G., Jingsui, Y., 2001. Oblique stepwise rise and growth of the Tibet Plateau. *Science* 294, 1671–1677.
- Taylor, M., Yin, A., 2009. Active structures of the Himalayan-Tibetan orogen and their relationships to earthquake distribution, contemporary strain field, and Cenozoic volcanism. *Geosphere* 5, 199–214.
- Taylor, M., Yin, A., Ryerson, F.J., Kapp, P., Ding, L., 2003. Conjugate strike-slip faulting along the Bangong-Nujiang suture zone accommodates coeval east-west extension and north-south shortening in the interior of the Tibetan Plateau. *Tectonics* 22. <http://dx.doi.org/10.1029/2002TC001361>.
- Tian, X., Wu, Q., Zhang, Z., Teng, J., Zeng, R., 2005. Joint imaging by teleseismic converted and multiple waves and its application in the INDEPTH-III passive seismic array. *Geophys. Res. Lett.* 32, L21315.
- Tian, X., Chen, Y., Tseng, T.-L., Klemperer, S.L., Thybo, H., Liu, Z., Xu, T., Liang, X., Bai, Z., Zhang, X., Si, S., Sun, C., Lan, H., Wang, E., Teng, J., 2015. Weakly coupled lithospheric extension in southern Tibet. *Earth Planet. Sci. Lett.* 430, 171–177.
- Tilmann, F., Ni, J., Team, I.I.S., 2003. Seismic imaging of the downwelling Indian lithosphere beneath central Tibet. *Science* 300, 1424–1427.
- Turner, S., Hawkesworth, C., Liu, J., Rogers, N., Kelley, S., van Calsteren, P., 1993. Timing of Tibetan uplift constrained by analysis of volcanic rocks. *Nature* 364, 50–54.
- Wessel, P., Smith, W.H.F., 1991. Free software helps map and display data. *EOS Trans. Amer. Geophys. U.* 72 (41), pp. 441, 445–446.
- Wei, S., Chen, Y.J., Sandvol, E., Zhou, S., Yue, H., Jin, G., Hearn, T.M., Jiang, M., Wang, H., Fan, W., Liu, Z., Ge, Z., Wang, Y., Feng, Y., Ni, J., 2010. Regional earthquakes in northern Tibetan Plateau: implications for lithospheric strength in Tibet. *Geophys. Res. Lett.* 37, L19307.
- Yang, H., Zhu, L., Chu, R., 2009. Fault-plane determination of the 18 April 2008 Mt. Carmel, Illinois, earthquake by detecting and relocating aftershocks. *Bull. Seismol. Soc. Am.* 99 (6), 3413–3420.
- Yin, A., 2000. Mode of Cenozoic east-west extension in Tibet suggesting a common origin of rifts in Asia during the Indo-Asian collision. *J. Geophys. Res.* 105 (B9), 21745–21759.
- Yin, A., Taylor, M.H., 2011. Mechanics of V-shaped conjugate strike-slip faults and the corresponding continuum mode of continental deformation. *Geol. Soc. Am. Bull.* 123, 1798–1821.
- Yin, J., Yao, H., Yang, H., Qin, W., Liu, J., Zhang, H., 2016. Frequency-dependent rupture process, stress change, and seismogenic mechanism of the 25 April 2015 Nepal Gorkha Mw 7.8 earthquake. *Sci. China Earth Sci.* <http://dx.doi.org/10.1007/s11430-016-9006-0>.
- Yuan, X., Ni, J., Kind, R., Mechie, J., Sandvol, E., 1997. Lithospheric and upper mantle structure of southern Tibet from a seismological passive source experiment. *J. Geophys. Res.* 102, 27491.
- Zhang, P., Shen, Z., Wang, M., Gan, W., Bürgmann, R., Molnar, P., Wang, Q., Niu, Z., Sun, J., Wu, J., Hanrong, S., Xinzhaoy, Y., 2004. Continuous deformation of the Tibetan Plateau from global positioning system data. *Geology* 32, 809–812.
- Zhao, L., Helmberger, D.V., 1991. Geophysical implications from relocations of Tibetan earthquakes; hot lithosphere. *Geophys. Res. Lett.* 18, 2205–2208.
- Zhao, L., Xie, X., He, J., Tian, X., Yao, Z., 2013. Crustal flow pattern beneath the Tibetan Plateau constrained by regional Lg-wave Q tomography. *Earth Planet. Sci. Lett.* 383, 113–122.
- Zhu, L., Helmberger, D.V., 1996. Intermediate depth earthquakes beneath the India-Tibet collision zone. *Geophys. Res. Lett.* 23, 435–438.